CHEMISTRY
A EUROPEAN JOURNAL

DOI: 10.1002/chem.201200248

Ferromagnetic Interactions in a 1D Alternating Linear Chain of π-Stacked 1,3-Diphenyl-7-(thien-2-yl)-1,4-dihydro-1,2,4-benzotriazin-4-yl Radicals

Christos P. Constantinides,[a, b] **Panayiotis A. Koutentis,***[a] **and Jeremy M. Rawson**[b]

Abstract: X-ray studies show that 1,3-diphenyl-7-(thien-2-yl)-1,4-dihydro-1,2,4-benzotriazin-4-yl (**6**) adopts a distorted, slipped π-stacked structure of centrosymmetric dimers with alternate short and long interplanar distances (3.48 and 3.52 Å). Cyclic voltammograms of 7-(thien-2-yl)benzotriazin-4-yl **6** show two fully reversible waves that correspond to the −1/0 and 0/+1 processes. EPR and DFT studies on radical **6** indicate that the spin density is mainly delocalized over the triazinyl fragment. Magnetic susceptibility measurements show that radical **6** obeys Curie–Weiss behavior in the 5–300 K region with $C = 0.378\ \mathrm{emu\,K\,mol^{-1}}$ and $\theta = +4.72$ K, which is consistent with ferromagnetic interactions between $S = \frac{1}{2}$ radicals. Fitting the magnetic susceptibility revealed the behavior is consistent with an alternating ferromagnetic chain ($g = 2.0071$, $J_1 = +7.12\ \mathrm{cm^{-1}}$, $J_2 = +1.28\ \mathrm{cm^{-1}}$).

Keywords: benzotriazinyls · heterocycles · magnetic properties · radicals · stacking interactions

Introduction

Persistent organic radicals have received increased attention as promising building blocks for functional molecular materials on account of their unique physical properties.[1] The presence of unpaired electrons in these organic molecules gives rise to bulk solid-state properties such as conductivity and magnetism that are traditionally associated with metals, their oxides, and ceramics.[2] Organic-based materials offer potential advantages over their inorganic counterparts since efficient and versatile organic synthesis facilitates the introduction of small structural changes that are needed to fine-tune properties.[2a]

Numerous families of stable radicals (verdazyl,[2d] nitroxide, nitronyl nitroxide radicals,[3a] heterocyclic thiazyl,[3b] selenazyl,[3c–e] and triphenylmethyl radicals[3f]) have been discovered and extensively studied. Nevertheless, benzotriazinyl radicals, which have been known since the late 1960s when Blatter et al. first prepared 1,3-diphenyl-1,4-dihydro-1,2,4-benzotriazin-4-yl (**1**) (Blatter's radical),[4] have been less investigated and only a few examples of this radical family have appeared in the literature.[5–9] On account of the ease of preparation and their exceptional air and moisture stability, benzotriazinyls have been recently revisited.[6–8]

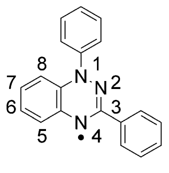

1

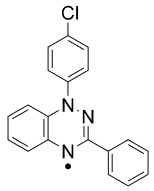

2

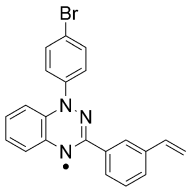

3

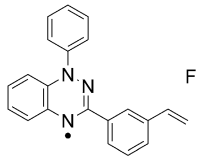

4

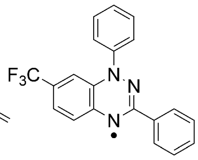

5

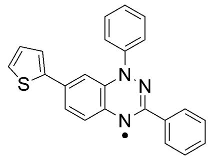

6

Their potential to functionalize at the 5-8 positions of the benzo-fused ring, as well as N1 of the triazinyl ring and C3, offers potential synthetic and structural diversity. Five derivatives have been previously reported with derivatives **1**, **2**, and **3** substituted at N1, and **4** functionalized at C3. Recently, we reported the first derivative functionalized at the benzo-fused ring **5**.

The magnetic properties of these benzotriazinyls prove interesting: whereas **2** exhibits short-range antiferromagnetic interactions[9] derivatives **3**–**5** demonstrate low-dimensional ferromagnetism.[7,8] Given the strict necessity for orbital orthogonality to propagate ferromagnetic exchange, the apparent propensity for radicals of this type to exhibit ferromagnetic interactions is unusual but seems to be intimately associated with the formation of slipped π-stacked structures[8] and has prompted us to prepare additional derivatives with a view to developing a better understanding of the effects of

---

[a] C. P. Constantinides, Dr. P. A. Koutentis
Department of Chemistry, University of Cyprus
P.O. Box 20537, 1678 Nicosia (Cyprus)
E-mail: koutenti@ucy.ac.cy

[b] C. P. Constantinides, Prof. J. M. Rawson
Department of Chemistry
The University of Cambridge
Lensfield Road, Cambridge, CB2 1EW (UK)

Supporting information for this article is available on the WWW under http://dx.doi.org/10.1002/chem.201200248.

substituents on crystal packing and ultimately magnetic behavior.

As part of this effort, we now report the synthesis and characterization of 1,3-diphenyl-7-(thien-2-yl)-1,4-dihydro-1,2,4-benzotriazin-4-yl (**6**) in which the thiophene group has the potential to generate favorable S⋅⋅⋅S contacts. Such S⋅⋅⋅S contacts play a key role in the packing and electronic properties of sulfur-rich organic conductors such as tetrathiafulvalene (TTF),[10a,b] and also oligo- and polythiophenes.[10c,d]

Results and Discussion

Synthesis and characterization: 1,2,4-Benzotriazinyl radicals are typically prepared by means of a five-step product-specific synthesis that affords the radicals in moderate yields and involves large excess amounts of HgO (toxic) or AgO (expensive) oxidants.[4,11] Recently, we developed a mild and high-yielding preparation of Blatter's radical **1** and several C7-substituted analogues through catalytic oxidation of the amidrazone precursors by using palladium-on-carbon and 1,8-diazabicyclo[5.4.0]undec-7-ene (DBU) in air.[6a] One of the analogues, 7-iodo-1,2,4-benzotriazinyl (**7**), can be further modified by means of Stille and Suzuki–Miyaura cross-coupling reactions to access a range of 7-aryl and 7-heteroaryl-1,2,4-benzotriazinyls.[6b] Both the Stille and Suzuki–Miyaura reactions are in most cases high yielding but the latter are cleaner; the former are faster but are accompanied by the benzotriazin-7(*H*)-one **8** as side product, which arises from the oxidation of the radical at C7 (Scheme 1). Blocking the C7 position with a trifluoromethyl group led to higher oxidative stability and, remarkably, when the 7-trifluoromethyl benzotriazinyl radical **5** was treated with an excess amount of MnO_2 or $KMnO_4$ in solutions of benzene heated at reflux, the radical was recovered unchanged.[7] The introduction of heteroaryl substituents at C7 can be doubly advantageous since they can inhibit formation of the benzotriazinone **8** and can also participate in various intermolecular interactions that can affect the packing of the radicals in the solid state. Radical **6** was considered a good candidate to study. Using our best conditions, thien-2-ylSnBu$_3$ (2 equiv) and Pd(OAc)$_2$ (5 mol%), radical **6** was prepared from **7** by means of Stille reaction conditions in 93% (Scheme 1).[6b]

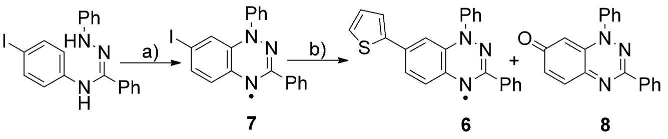

Scheme 1. Synthesis of 7-thien-2-ylbenzotriazinyl **6**. a) DBU (0.1 equiv), Pd/C (1.6 mol%), CH_2Cl_2 (1 mL), approximately 20°C under an air atmosphere, 4–9 h (81%);[6a] b) Pd(OAc)$_2$ (5 mol%), thien-2-ylSnBu$_3$ (2 equiv), dry DMF (2 mL), approximately 100°C, under argon, 30 min (93%).[6b]

X-ray studies: Suitable single crystals of **6** for X-ray diffraction studies (Table S1 in the Supporting Information) were obtained by slow evaporation of a concentrated hexane solution. Radical **6** crystallizes in the monoclinic space group $P2_1/n$ with one molecule in the asymmetric unit. To date, crystal structures of benzotriazinyl radicals **1**–**5** have been reported and the molecular geometry of **6** is described in relation to **1**–**5**.

The 1,2,4-amidrazonyl moiety in radical **6** is almost planar with a deviation from planarity of approximately 3.5° as defined by the angle measured between the plane of the N1, N2, C1, N3 amidrazonyl atoms and the plane of the fused phenyl ring (Figure 1). This is similar to radicals **1**, **2**, and **4**, which are planar and also radical **3** (6.8°) but markedly less than radical **5** (14.5°).

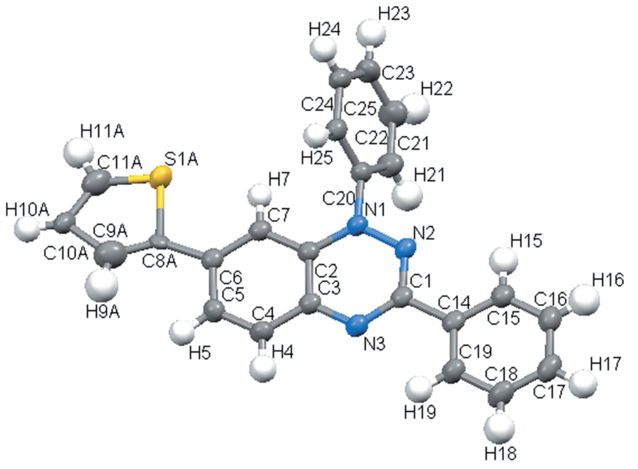

Figure 1. Ellipsoid diagram of radical **6** in the crystal with atom-numbering scheme (180° disorder of the thienyl group about the C6–C8 bond has been removed for clarity).

The C–N bond lengths of radical **6** (C1–N2 1.336(2) Å, C1–N3 1.337(2) Å) are intermediate between typical single and double C–N bonds. The C1-N2-N1 and C1-N3-C3 angles of 115.0(1) and 116.0(1)°, respectively, are typical of sp^2-hybridized pyridine coordination complexes.[12] Radical **6** shows bond lengths and angles similar to radicals **1**–**5**, which is consistent with a strong delocalization within the amidrazoyl moiety of the heterocycle.

The torsion angle (C21-C20-N1-N2) of the *N*-phenyl group with respect to the plane of the benzotriazinyl is 60.1(2)° as a result of steric interactions between the *peri*-hydrogen H25 and the phenyl *ortho*-hydrogen H7. In contrast, the phenyl substituent at C1 is essentially coplanar (torsion C19-C14-C1-N3 0.8(2)°) with the benzotriazinyl ring affording two favorable but weak intramolecular hydrogen bonds (C15⋅⋅⋅N2 2.805(2) Å, C19⋅⋅⋅N3 2.772(2) Å). The 2-thienyl substituent is nearly coplanar with the benzotriazinyl group (≈6.6°) but is disordered over two sites in a 50:50 ratio by a 180° rotation about the C6–C8 bond.

The packing of radical **6** comprises a centrosymmetric dimer linked through a pair of crystallographically equiva-

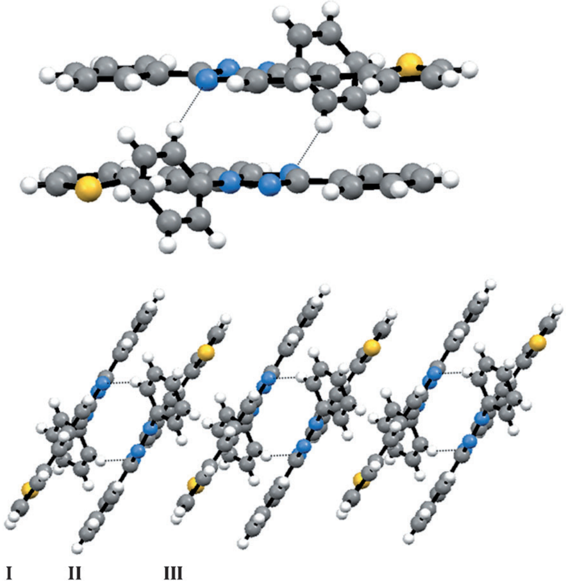

Figure 2. Solid-state structure of **6**. Top: Close intermolecular C–H···N contacts lead to a face-to-face interaction between benzotriazinyl radicals in **6**. Bottom: Stacking of radicals parallel to the *b* axis. Labels I, II and III refer to molecules discussed in the text.

lent C–H···N contacts between a triazinyl N (at position N4) and an *ortho*-hydrogen atom of the *N*-phenyl ring ($d_{\text{C}\cdots\text{N}}$ 3.630(2) Å; Figure 2, top). These dimers pack parallel to the crystallographic *b* axis (Figure 2, bottom), thus leading to a π-stacked structure with close contacts in the range 3.5–3.8 Å between delocalized π systems. Notably, both **3** and **4** exhibit intra-stack *ortho*-C–H···N interactions but to position N2 of a neighboring triazinyl radical (see the Supporting Information).

The interplanar distance between the weakly hydrogen-bonded pair of molecules (I–II, Figure 2, bottom) is 3.52 Å with a slippage angle of $\phi_2 = 15.7°$, whereas the interplanar distance between molecules in radical pair II–III is 3.48 Å with a slippage angle of $\phi_1 = 45.9°$. As such, the column can be envisaged as a slipped stack of radical pairs and can be considered electronically to be a 1D Peierls distorted stack of radicals with alternating interplanar distances.

The crystal packing of radical **6** shares similar features with the packing of other benzotriazinyl radicals **2**–**5** in that all adopt a π-stacked motif. However, whereas radicals **3**–**5** form regular 1D chains through simple translation and have shorter interplane distances, both **2** and **6** incorporate an additional symmetry element in addition to translation. For radicals **3**–**5** the interplanar distances are 3.34, 3.46, and 3.35 Å and have slippage angles of 36, 46, and 28°, respectively, with favorable edge-to-face (**3** and **5**) and face-to-face (**4**) π–π interactions between the *N*-phenyl groups. Such contacts are absent from the packing of radicals **2** and **6** in which the molecules are related by a center of inversion that resides at the centre of their radical-pair structure.

The presence of disorder in the 2-thienyl group would suggest that the structure-directing influence of the S atom is negligible (or at least the possible interactions it adopts in the two orientations are near equi-energetic). It is notable, however, that the thienyl ring is nearly coplanar with the phenyl ring so as to optimize efficient π stacking of the molecules along the *b* axis. In addition, twisting of the thienyl ring from planarity would require a disruption to the planarity of the phenyl ring in a neighboring molecule in the same π stack that exhibits the intramolecular C–H···N interactions already described.

Neighboring columns in radical **6** are connected through a net of contacts (S···S 3.36 Å, S···H5 2.86 Å, and H25···H25′ 2.39 Å) that link adjacent radicals in a tail-to-tail manner to form 2D sheets along the *a* axis (Figure S1 in the Supporting Information). These sheets pack in a parallel arrangement along the *ac* diagonal plane (Figure S2 in the Supporting Information) and in a herringbone mode down the *a* axis. (Figure S3 in the Supporting Information).

Cyclic voltammetry and EPR spectroscopy: The redox behavior of radical **6** is similar to radicals **1**–**5** in that it exhibits two fully reversible waves that correspond to the −1/0 and 0/+1 processes (Figure 3). With oxidation potentials occurring between +0.10 to +0.36 V versus ferrocene/ferrocenium (Fc/Fc$^+$; Table S2 in the Supporting Information), benzotriazinyls can act as good electron donors in charge-transfer salts. Blatter's radical **1** forms a charge-transfer salt with 7,7,8,8-tetracyanoquinodimethane (TCNQ), which is a pressure-dependent semiconductor.[13]

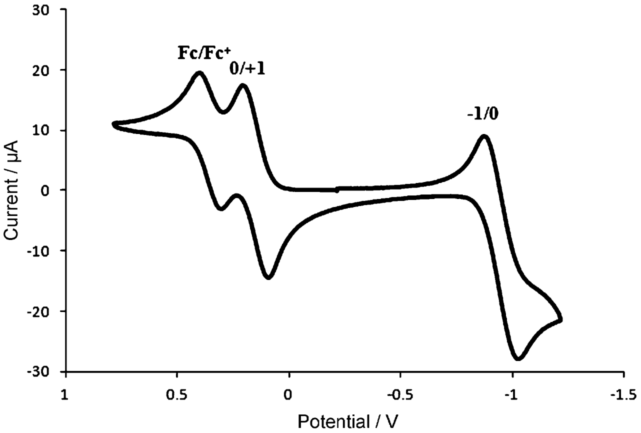

Figure 3. Cyclic voltammogram of **6** (1 mM). Conditions: $n\text{Bu}_4\text{NBF}_4$ 0.1 M, CH_2Cl_2, RT, 50 mV s^{-1}.

Although radical **6** has an electron-donating group attached at C7, a ring position with substantial contribution to the singly occupied molecular orbital (SOMO), its oxidation potential (+0.15 V) is slightly higher than that of Blatter's radical **1** (+0.1 V) but less than those of radicals **4** (+0.21 V) and **3** (+0.25 V), which have substituents not directly connected to the benzotriazinyl ring. In contrast, radical **5** with an electron-withdrawing CF_3 substituent at C7 has a slightly higher oxidation potential (+0.36 V) on account of the electronegative nature of this group. Although benzotriazinyls have an extended delocalized benzo-fused structure relative to verdazyls,[14] one less N atom in their ring leads to higher oxidation potentials. However, benzotriazinyls have lower reduction potentials than verdazyls but significantly higher than their isoelectronic benzothiadiazinyls, which reduce easily to give benzothiadiazines.[15] The cell potentials for the two nitrogen-rich radical families have a similar value of around 1.0 V, which is larger than those found for other neutral radical families (e.g., thiazyls)[2b,3b] that have been investigated as promising building blocks for conducting materials.

EPR studies on radical **6** revealed hyperfine coupling constants (hfcc) similar to radicals **1**–**5** (Table S3 in the Supporting Information). The solution EPR spectrum of radical **6** (Figure 4) exhibits a seven-line spectrum that is consistent with the coupling of the unpaired electron with the three similar but slightly inequivalent ^{14}N nuclei. EPR spectra recorded in both first- (Figure 4) and second-derivative modes (Figure S5 in the Supporting Information) were simulated to determine the hyperfine coupling constants. By comparison with previous studies,[6b,8,11a] the largest hfcc was assigned to N1 (7.38 G), with the hfcc to N2 tentatively assigned to be slightly larger than that to N3 (4.92 and 4.59 G, respectively).

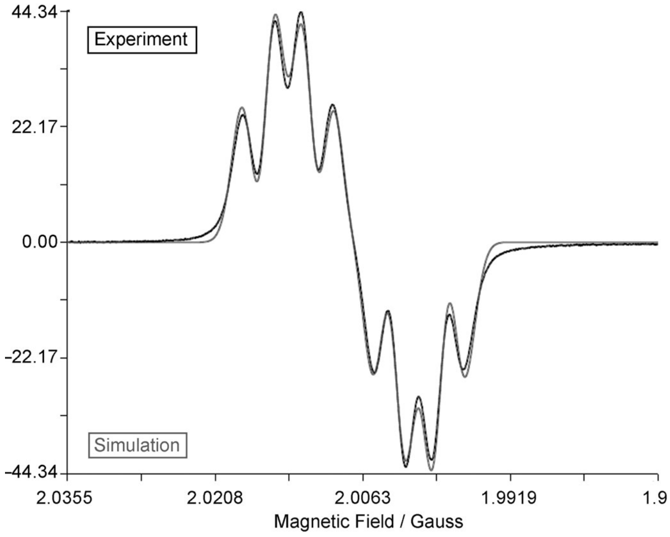

Figure 4. Experimental and simulated EPR spectrum of radical **6** at RT in CH_2Cl_2. Fitting parameters: $g=2.0071$, $a_N(1)=7.38$, $a_N(2)=4.92$, $a_N(3)=4.59$ (lineshape: $\Delta H_{pp}\approx 2$ G; 100% Gaussian).

Atomic spin densities of the benzo-fused ring in radical **6** could not be experimentally determined since line broadening of the spectrum resulted in poor resolution of the hyperfine coupling to hydrogen atoms. Electron nuclear double resonance (ENDOR) studies on the Blatter radical **1** performed by Neugebauer and co-workers reported the magnitude and the sign of the hyperfine coupling constants of the hydrogen and nitrogen atoms.[16] Based on these numbers, we employed the McConnell equation[17] to estimate the spin-density distribution around the benzotriazinyl ring for radical **1** and compared it to that of radical **6**.

It is clear from Table 1 that most of the spin density resides on the triazinyl ring and radical **6** has similar spin-density values for the three nitrogen nuclei to radical **1**. The ENDOR measurements on **1** indicate the presence of small quantities of negative spin density delocalized over the benzo-fused ring. DFT calculations at the UB3LYP/6-311+G(d,p) level of theory on radical **6** failed to predict the magnitude and the sign of experimentally estimated spin densities in accordance with previous studies, and this was attributed to the fact that DFT methods do not describe the electronic structure of the ground state correctly.[7,8]

Table 1. Spin densities (ρ) estimated from hyperfine coupling constants using McConnell's equation.[a]

Radical	N1	N2	N3	C4	C5	C6	C7
1	+0.300	+0.238	+0.225	−0.049	−0.043	−0.067	−0.032
6	+0.295	+0.232	+0.216	–	–	–	–

[a] $A_H=Q_H\cdot\rho_C$ and $A_N=Q_N\cdot\rho_N$, in which A_H, A_N are the hfc in Gauss; $Q_H=(-)27.3$ G,[17] $Q_N=21.2$ G[18] (for N2 and N3), and $Q_N=25$ G[18a,b] (for N1).

Magnetic properties: 1,2,4-Benzotriazinyls are a fertile source of interesting magnetic properties. Although few radicals of this family have appeared so far in the literature, the majority exhibit short-range ferromagnetic interactions. Radicals **3**–**5** exhibit 1D Heisenberg linear chain ferromagnetism with intrachain exchange interactions of $J=+7.38$,[7] +6.90, and +1.05 cm^{-1}, respectively.[8] Conversely, radical **2** exhibits strong antiferromagnetic interactions that are modeled as an alternating linear chain with magnetic exchange parameters of $J_1=-76.50$ cm^{-1}, $J_2=-22.90$ cm^{-1}, and an alternation parameter of $a=J_2/J_1=0.3$.[9] We were therefore interested to examine the magnetic behavior of **6**.

The variable-temperature magnetic susceptibility of radical **6** was measured using a Quantum Design SQUID magnetometer in the region 5–300 K in an applied field of 0.5 T. The data were corrected for both sample diamagnetism (Pascal's constants) and the diamagnetism of the sample holder.

Radical **6** obeys Curie–Weiss behavior down to 5 K (Figure 5, inset) with $C=0.378$ emu K mol^{-1}, which corresponds to an $S=\frac{1}{2}$ radical with $g=2.0071$, consistent with that measured in solution by EPR spectroscopy. The Weiss constant ($\theta=+4.72$ K) is consistent with local ferromagnetic interactions.

Attempts to model the magnetism of **6** using the Bleaney–Bowers equation[19] [Eq. (1)] for an isolated dimer of $S=\frac{1}{2}$ radicals (based on the Hamiltonian $\mathscr{H}=-2J_1\hat{S}_1\hat{S}_2$) rapidly revealed that interdimer interactions were required to model the low-temperature values of χT that surpass the value of 0.5 emu K mol^{-1} per monomer that is anticipated

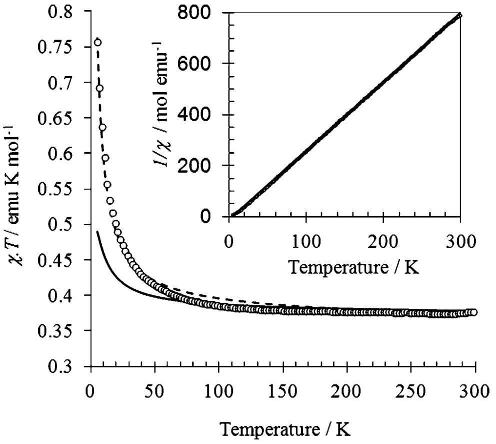

Figure 5. Temperature dependence of χT for radical **6**. The dashed line represents the best fit to the 1D ferromagnetic linear chain model ($g = 2.0071$, $J = +4.2\ \text{cm}^{-1}$), the solid line represents the corresponding fit to an isolated $S = 1/2$ dimer with $g = 2.0071$ and $J_1 = +6.6\ \text{cm}^{-1}$, illustrating the requirement for a ferromagnetic interdimer exchange term. Inset: Curie–Weiss behavior in the 5–300 K region ($C = 0.378\ \text{emu K mol}^{-1}$, $\theta = +4.72$ K).

for a ferromagnetic interaction between $S = 1/2$ spins at temperatures below 19 K.

$$\chi = \frac{Ng^2\beta^2}{k(T-\theta)}\frac{1}{[3+\exp(-2J_1/kT)]} \qquad (1)$$

Inclusion of a mean field term (θ) to model interdimer ferromagnetic exchange provided a much improved fit with $g = 2.0071$ (fixed), $J_1 = +6.6\ \text{cm}^{-1}$, and $\theta = +1.75$ K, in which J_1 is the intradimer interaction. Within the mean field approximation, the mean field term (θ) correlates to the interdimer interactions according to Equation (2):

$$\theta = 2zJ_2S(S+1)/3k \qquad (2)$$

By assuming the dominant magnetic exchange interaction occurs through π^*–π^* interactions along the π-stacking direction ($z = 2$), we can estimate a mean interdimer interaction, J_2 of $+1.2\ \text{cm}^{-1}$. The mean of the intra- and interdimer exchange parameters $+3.9\ \text{cm}^{-1}$ ($+5.6$ K) is consistent with the observed Weiss constant. However, the similar magnitude of intra- and interdimer exchange interactions ($J_2/J_1 = 0.18$) suggests that the dimer model does not adequately represent the behavior of **6**. Given the inadequacies of the dimer model, we sought to model the behavior of **6** based on a one-dimensional chain, which corresponds to the π-stacking direction in which orbital overlap and hence magnetic exchange between radicals is likely to be most efficient. Whereas there are models for alternating antiferromagnetically coupled chains ($J_1 < J_2 < 0$) of $S = 1/2$ ions and alternating ferro-/antiferromagnetically coupled chains ($J_1 < 0 < J_2$), there is a dearth of literature that describes the magnetism of alternating ferromagnetically coupled chains ($J_1 > J_2 > 0$) for $S = 1/2$ ions. In cases in which at least one of the exchange interactions in the chain is antiferromagnetic, then there is a turning point in χ versus T.[20] This corresponds to a minimum when $J_1 < 0 < J_2$ and a maximum when $J_1 < J_2 < 0$. Both the position and value of the turning point in $\chi(T)$ is sensitive to the relative signs and magnitudes of J_1 and J_2. Conversely, for an alternating ferromagnetic chain ($J_1 > J_2 > 0$) χ versus T continues to increase monotonically with decreasing temperature. Curve-fitting of such functions is likely to be rather insensitive to the values of J_1 and J_2, and these two parameters are likely to be strongly correlated. To probe the magnetism of **6** further, we investigated a regular ferromagnetic chain of $S = 1/2$ spins using Baker's high-temperature series expansion [Eq. (3)][21] to estimate the mean value of J:

$$\chi = \frac{Ng^2\beta^2}{4kT}[N/D]^{2/3} \qquad (3)$$

in which $N = 1 + 5.7979916x + 16.902653x^2 + 29.376885x^3 + 29.832959x^4 + 14.036918x^5$ and $D = 1 + 2.7979916x + 7.008678x^2 + 8.6538644x^3 + 4.5743114x^4$, and $x = J/2kT$.

Fitting the magnetic data to Equation (3) yielded $J = +4.2\ \text{cm}^{-1}$ in good agreement with the mean value estimated from the dimer model with interdimer interactions ($+3.9\ \text{cm}^{-1}$). By applying the ratio of J_1/J_2 from the dimer model to the one-dimensional chain, we determined estimated J_1 and J_2 values along the chain direction of $+7.12$ and $+1.28\ \text{cm}^{-1}$, respectively.

Discussion

Although DFT studies on **6** based on a single-point calculation (UB3LYP/6-311+G(d,p)) performed on the X-ray geometry coordinates do not describe accurately the electronic structure of the ground state, they confirm the π character of the radical (Figure 6) with most of the orbital density being confined on the benzotriazinyl ring.

Since the SOMO of **6** is of π character, we anticipate the strongest SOMO–SOMO interactions to correspond to the π-stacking direction, that is, parallel to the b axis. The crys-

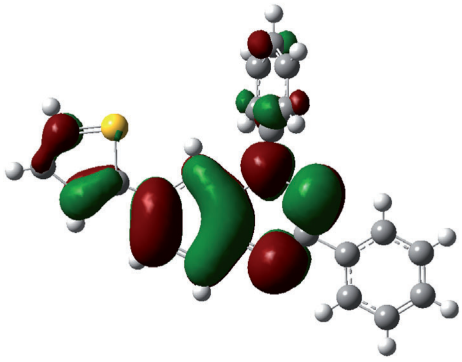

Figure 6. Singly occupied molecular orbital of **6** calculated at the UB3LYP/6-311+G(d,p) level of theory.

tal structure reveals two types of radical•••radical contacts parallel to the stacking direction (Figure 2). We define the staggered radical pair within the stack as dimer II–III and the near-eclipsed pair as dimer I–II, thus leading to two different exchange parameters J_1 and J_2 along the stacking direction. Normally, the magnitude of the exchange interaction can be estimated by computing the energy of the triplet and broken-symmetry singlet for pairs of radicals.[22] However, this relies on a basis set and functional that accurately reproduce the spin-density distribution of the isolated radical. Whereas the current studies confirm the π* nature of the singly occupied orbital, significant discrepancies between the calculated and estimated (from EPR) spin-density distributions caution against such an approach being reliable in this case. Such problems with accurately reproducing the spin distribution in these triazinyls have been noted previously and indicate the requirement for a multiconfigurational approach.[8] Such approaches are significantly more computationally expensive, and examining a pair of radicals is currently prohibitive. Instead we have applied a more qualitative approach to understand the behavior of **6**.

According to the McConnell-I model,[23] atoms with positive spin density are exchange-coupled to atoms with negative spin density in neighboring molecules to give ferromagnetic coupling ($H^{AB} = -S^{A}\cdot S^{B}\Sigma J_{ij}^{AB}\rho_i^{A}\rho_j^{B}$). In **6**, the eclipsed centrosymmetric radical pair I–II leads to the triazinyl moieties of one radical located above the benzo-fused ring of the other radical and vice versa. Since the spin density on the triazinyl ring is predominantly positive but negative on the benzo-fused ring (Table 1), this arrangement is anticipated to favor a ferromagnetic interaction.

In the molecular orbital model,[24] the exchange coupling interaction ($J_{AB} = 2k_{ij} + 4c_{ij}S_{ij}^{2}$) is proportional to the size of the overlap between SOMO orbitals (S_{ij}), which depends on the distance and orientation of the interacting radicals. When the two interacting SOMO orbitals are orthogonal to each other, S_{ij} is zero and the exchange coupling interaction is ferromagnetic. A qualitative analysis of the SOMO orbitals of radical pairs I–II and II–III of radical **6** indicates that in radical pair II–III the orthogonality is more pronounced due to the greater slippage of the radicals ($\phi_1 = 45.9°$) (Figure 7).

The benzotriazinyl moiety, which bears most of the orbital density (and hence spin density), is located on top of the adjacent thien-2-yl substituent that bears little orbital density. The radical pair II–III of radical **6** has the same interplanar distance and slippage angle (3.48 Å, $\phi_1 = 45.9°$) as the 1D π-stacked molecules of radical **4** (3.46 Å and $\phi = 46°$). The crystal packing of radical **4** is comprised exclusively of these slipped π-stacked molecules that interact between them, and that interaction was ferromagnetic ($J = +6.90\ \mathrm{cm}^{-1}$),[8] which is not dissimilar to that estimated from our analysis of the magnetic susceptibility of **6** ($+7.12\ \mathrm{cm}^{-1}$). The radical pair I–II is less slipped than II–III; the commencement of some overlap of regions of positive spin density may lead to a weakening of the ferromagnetic interaction or indeed ultimately make it antiferromagnetic. However, whereas this pair is substantially closer to eclipsed ($\phi_2 = 15.7°$), the interplane separation is simultaneously increased (3.52 versus 3.48 Å in dimer II–III), which leads to reduced orbital overlap. As a consequence, we assign this second interaction to the weaker ferromagnetic interaction, $+1.28\ \mathrm{cm}^{-1}$).

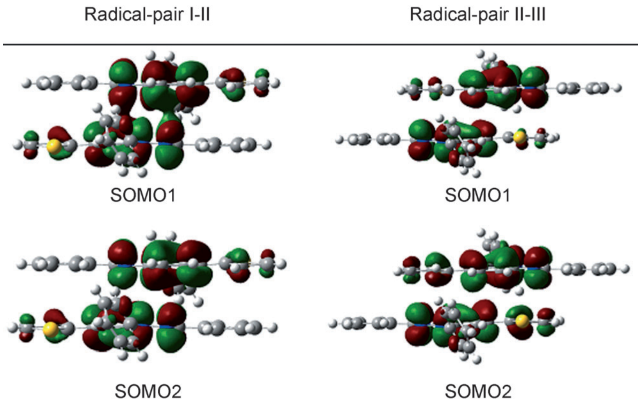

Figure 7. SOMO orbitals of radical pairs I–II and II–III for radical **6** calculated at the UB3LYP/6-311+G(d,p) level of theory.

Conclusion

The crystal structure and the magnetic properties of 1,3-diphenyl-7-(thien-2-yl)-1,4-dihydro-1,2,4-benzotriazin-4-yl (**6**) have been investigated. The radicals π-stack in one-dimensional columns along the *b* axis and comprise slipped radical pairs (I–II and II–III) with alternate short and long interplanar distances. Magnetic susceptibility measurements reveal the existence of weak ferromagnetic interactions within the 1D stacks. Spin-density distributions determined by EPR spectroscopy, SOMO orbitals computed using DFT methods, and a magneto-structural model have allowed us to correlate the estimated exchange interactions to different dimer pairs within the distorted π stack; $J_2 = +1.28\ \mathrm{cm}^{-1}$ and $J_1 = +7.12\ \mathrm{cm}^{-1}$, which correspond to the radical pairs I–II and II–III, respectively. The slippage of radicals along the stacking direction causes the orthogonality of the SOMO orbitals of the radical pairs. Elegant studies by Oakley and co-workers on heavier p-block radicals have shown that the nature of the magnetic exchange along the π-stacking direction is sensitive to the degree of slippage and can be controlled by fine-tuning the steric properties of the substituents.[3c] Further modifications to the benzotriazinyl framework are in progress to optimize both the intradimer separation and the degree of slippage.

Experimental Section

Synthetic procedures: The synthesis and characterization of radical **6** can be found in the Supporting Information.

Instrumental analyses: Cyclic voltammetry (CV) measurements were performed using a Princeton Applied Research Potentiostat/Galvanostat

263A apparatus. The concentration of the benzotriazinyl radical used was 1 mM in CH_2Cl_2. A 0.1 M solution of tetrabutylammonium tetrafluoroborate ($TBABF_4$) in CH_2Cl_2 was used as electrolyte. The reference electrode was Ag/AgCl and the scan rate was $50\,mV\,s^{-1}$. Ferrocene was used as an internal reference; the $E_{1/2}$(ox) of ferrocene in this system was 0.352 V.[25] EPR measurements were carried out using a Bruker EMX spectrometer using an X-Band (9.8 GHz) microwave bridge at 290 K. The EPR spectrum was simulated using the Winsim Spectral Simulation for MS Windows 9*x*, NT v0.98.[26] Magnetic susceptibility measurements were performed using a Quantum Design MPMS-XL SQUID magnetometer in the temperature region of 5–300 K and in an applied magnetic field of 5000 G. X-ray diffraction data were collected using a Nonius Kappa-CCD diffractometer, equipped with a CCD area detector and graphite-monochromated $Mo_{K\alpha}$ radiation ($\lambda = 0.71073$ Å). A suitable crystal (black plate of dimensions $0.32 \times 0.18 \times 0.10$ mm) was attached to a glass fiber using paratone-N oil and transferred to a goniometer where it was cooled to 180(2) K for data collection using an Oxford Instruments cryostream. Unit-cell dimensions were determined and refined using 17991 ($1.02 < \theta < 27.48°$), reflections. An empirical absorption correction was applied using a multiscan method based on symmetry-related measurements using Sortav.[27] The structure was solved by direct methods and refined on F^2 using full-matrix least squares using SHELXL97.[28] Programs used: HKL Denzo and Scalepack for cell refinement and data reduction[29a] and MERCURY[29b] for molecular graphics. The non-hydrogen atoms were treated anisotropically, whereas the hydrogen atoms were placed in calculated ideal positions and refined by using a riding model. The thienyl group was found to be disordered over two positions. The site occupancy factors (sof's) of the two orientations were determined by isotropic refinement with common U_{iso} for chemically equivalent atoms in each fragment to afford a ratio of 0.493:0.507. Subsequent anisotropic refinement of the thienyl groups in the latter stages of refinement used fixed sof's of 0.5 for the two orientations. Unit-cell data and structure refinement details are listed in Table S1 in the Supporting Information. Full details can be found in the CIF file provided in the Supporting Information.

Computational methods: Single-point calculations at the UB3LYP level of theory with the higher-level basis set of 6-311+G(d,p) were carried out on the X-ray geometry of radical **6** to calculate the SOMO orbitals of the radical pairs I–II and II–III. The above computation was performed by using the Gaussian 03 suite of programs.[30]

Acknowledgements

We thank the University of Cyprus (medium-sized grants), the Cyprus Research Promotion Foundation (grant no. ΥΓΕΙΑ/ΒΙΟΣ/0308(ΒΙΕ)/13) and the following organizations in Cyprus for generous donations of chemicals and glassware: the State General Laboratory, the Agricultural Research Institute, the Ministry of Agriculture and Biotronics Ltd. Furthermore, we thank the A.G. Leventis Foundation for helping to establish the NMR spectroscopic facility in the University of Cyprus. We thank Dr. John Davies (University of Cambridge) for the collection of the crystallographic data.

---

[1] a) *Magnetic Properties of Organic Materials* (Ed.: P. M. Lahti), Marcel-Dekker, New York, **1999**; b) *Molecular Magnetism: New Magnetic Materials* (Eds.: K. Itoh, M. Kinoshita), Kodansha and Gordon & Breach, Tokyo, **2000**.

[2] a) I. Ratera, J. Veciana, *Chem. Soc. Rev.* **2012**, *40*, 303–349; b) D. A. Haynes, *CrystEngComm* **2011**, *13*, 4793–4805; c) O. A. Rakitin, *Russ. Chem. Rev.* **2011**, *80*, 647–659; d) R. G. Hicks, *Org. Biomol. Chem.* **2007**, *5*, 1321–1338.

[3] a) S. Nakatsuji, H. Anzai, *J. Mater. Chem.* **1997**, *7*, 2161–2174; b) J. M. Rawson, A. Alberola, A. Whalley, *J. Mater. Chem.* **2006**, *16*, 2560–2575; c) M. Mito, Y. Komorida, H. Tsuruda, J. S. Tse, S. Desgreniers, Y. Ohishi, A. A. Leitch, K. Cvrkalj, C. M. Robertson, R. T. Oakley, *J. Am. Chem. Soc.* **2009**, *131*, 16012–16013; d) C. M. Robertson, A. A. Leitch, K. Cvrkalj, D. J. T. Myles, R. W. Reed, P. A. Dube, R. T. Oakley, *J. Am. Chem. Soc.* **2008**, *130*, 14791–14801; e) A. A. Leitch, J. L. Brusso, K. Cvrkalj, R. W. Reed, C. M. Robertson, P. A. Dube, R. T. Oakley, *Chem. Commun.* **2007**, 3368–3370; f) A. Rajca, *Chem. Rev.* **1994**, *94*, 871–893.

[4] H. M. Blatter, H. Lukaszewski, *Tetrahedron Lett.* **1968**, *9*, 2701–2705.

[5] a) C. Krieger, F. A. Neugebauer, *Acta Crystallogr.* **1996**, *C52*, 3124–3126; b) A. T. Gubaidullin, B. I. Buzykin, I. A. Litvinov, N. G. Gazetdinova, *Russ. J. Gen. Chem.* **2004**, *74*, 939–943.

[6] a) P. A. Koutentis, D. Lo Re, *Synthesis* **2010**, 2075–2079; b) C. P. Constantinides, P. A. Koutentis, G. Loizou, *Org. Biomol. Chem.* **2011**, *9*, 3122–3125.

[7] C. P. Constantinides, P. A. Koutentis, H. Krassos, J. M. Rawson, A. J. Tasiopoulos, *J. Org. Chem.* **2011**, *76*, 2798–2806.

[8] B. Yan, J. Cramen, R. McDonald, N. L. Frank, *Chem. Commun.* **2011**, *47*, 3201–3203.

[9] K. Mukai, K. Inoue, N. Achiwa, J. B. Jamali, C. Krieger, F. A. Neugebauer, *Chem. Phys. Lett.* **1994**, *224*, 569–575.

[10] a) J. J. Novoa, M. C. Rovira, C. Rovira, J. Veciana, J. Tarrés, *Adv. Mater.* **1995**, *7*, 233–237; b) C. Rovira, J. J. Novoa, *Chem. Eur. J.* **1999**, *5*, 3689–3697; c) A. Gavezzotti, G. Filippini, *Synth. Met.* **1991**, *40*, 257–266; d) D. Fichou, *J. Mater. Chem.* **2000**, *10*, 571–588.

[11] a) F. A. Neugebauer, I. Umminger, *Chem. Ber.* **1980**, *113*, 1205–1225; b) H. M. Blatter, US Pat. 3 423 409, **1969**; c) R. Huisgen, J. Wolf, *Chem. Ber.* **1969**, *102*, 1848–1858; d) F. A. Neugebauer, I. Umminger, *Chem. Ber.* **1981**, *114*, 2423–2430.

[12] a) G. J. Gainsford, A. D. Woolhouse, *Aust. J. Chem.* **1980**, *33*, 2447–2454; b) R. R. Schmidt, *Angew. Chem.* **1975**, *87*, 603–613; *Angew. Chem. Int. Ed. Engl.* **1975**, *14*, 581–591; c) R. N. Butler, A. M. Evans, E. M. McNeela, G. A. O'Haloran, P. D. O'Shea, D. Cunningham, P. McArdle, *J. Chem. Soc. Perkin Trans. 1* **1990**, 2527–2536.

[13] a) K. Hutchison, G. Srdanov, R. Menon, J.-C. Gabriel, B. Knight, F. Wudl, *J. Am. Chem. Soc.* **1996**, *118*, 13081–13082; b) K. Hutchison, G. Srdanov, R. Menon, J.-C. Gabriel, B. Knight, F. Wudl, *Synth. Met.* **1997**, *86*, 2147–2148.

[14] J. B. Gilroy, S. D. J. McKinnon, B. D. Koivisto, R. G. Hicks, *Org. Lett.* **2007**, *9*, 4837–4840 and references therein.

[15] J. Zienkiewicz, P. Kaszynski, V. G. Young, *J. Org. Chem.* **2004**, *69*, 7525–7536.

[16] F. A. Neugebauer, G. Rimmler, *Magn. Reson. Chem.* **1988**, *26*, 595–600.

[17] H. M. McConnell, *J. Chem. Phys.* **1958**, *28*, 1188–1192.

[18] a) D. J. Singel, W. A. J. A. van der Poel, J. Schmidt, J. H. van der Waals, R. de Beer, *J. Chem. Phys.* **1984**, *81*, 5453–5461; b) S. Stoll, Y. N. Jahromy, J. J. Woodward, A. Ozarowski, M. A. Marletta, R. D. Britt, *J. Am. Chem. Soc.* **2010**, *132*, 11812–11823; c) J. Luzon, J. Campo, F. Palacio, G. J. McIntyre, J. M. Rawson, R. J. Less, C. M. Pask, A. Alberola, R. D. Farley, D. M. Murphy, A. E. Goeta, *Phys. Rev. B* **2010**, *81*, 144429-1—144429-12.

[19] B. Bleaney, K. D. Bowers, *Proc. R. Soc. London, Ser. A* **1952**, *214*, 451–465.

[20] For example, see: O. Kahn, *Molecular Magnetism*, Wiley-VCH, Weinheim, **1993**.

[21] G. A. Baker Jr., G. S. Rushbrooke, H. E. Gilbert, *Phys. Rev.* **1964**, *135*, A1272–1277.

[22] J. J. Novoa, M. Deumal, J. Jornet-Somoza, *Chem. Soc. Rev.* **2011**, *40*, 3182–3212.

[23] H. M. McConnell, *J. Chem. Phys.* **1963**, *39*, 1910–1911.

[24] M. Deumal, J. J. Novoa, M. J. Bearpark, P. Celani, M. Olivucci, M. A. Robb, *J. Phys. Chem. A* **1998**, *102*, 8404–8412.

[25] M. Dietrich, J. Heinze, *J. Am. Chem. Soc.* **1990**, *112*, 5142–5145.

[26] Public EPR Software Tools: Winsim Spectral Simulation for MS-Windows 9x, NT v0.98, D. A. O'Brien, D. R. Duling, Y. C. Fann, NIEHS, National Institute of Health, USA.

[27] Bruker AXS SORTAV, R. H. Blessing, *Acta. Cryst.* **1995**, *A51*, 33–38.

[28] G. M. Sheldrick, SHELXL97, University of Göttingen, Germany.

[29] a) HKL Scalepack, Z. Otwinski, W. Minor, *Methods in Enzymol.* **1997**, *A276*, 307–326; b) C. F. Macrae, P. R. Edgington, P. McCabe, E. Pidcock, G. P. Shields, R. Taylor, M. Towler, J. van de Streek, *J. Appl. Crystallogr.* **2006**, *39*, 453–457.

[30] Gaussian 03, Revision C.02, M. J. Frisch, G. W. Trucks, H. B. Schlegel, G. E. Scuseria, M. A. Robb, J. R. Cheeseman, J. A. Montgomery, Jr., T. Vreven, K. N. Kudin, J. C. Burant, J. M. Millam, S. S. Iyengar, J. Tomasi, V. Barone, B. Mennucci, M. Cossi, G. Scalmani, N. Rega, G. A. Petersson, H. Nakatsuji, M. Hada, M. Ehara, K. Toyota, R. Fukuda, J. Hasegawa, M. Ishida, T. Nakajima, Y. Honda, O. Kitao, H. Nakai, M. Klene, X. Li, J. E. Knox, H. P. Hratchian, J. B. Cross, V. Bakken, C. Adamo, J. Jaramillo, R. Gomperts, R. E. Stratmann, O. Yazyev, A. J. Austin, R. Cammi, C. Pomelli, J. W. Ochterski, P. Y. Ayala, K. Morokuma, G. A. Voth, P. Salvador, J. J. Dannenberg, V. G. Zakrzewski, S. Dapprich, A. D. Daniels, M. C. Strain, O. Farkas, D. K. Malick, A. D. Rabuck, K. Raghavachari, J. B. Foresman, J. V. Ortiz, Q. Cui, A. G. Baboul, S. Clifford, J. Cioslowski, B. B. Stefanov, G. Liu, A. Liashenko, P. Piskorz, I. Komaromi, R. L. Martin, D. J. Fox, T. Keith, M. A. Al-Laham, C. Y. Peng, A. Nanayakkara, M. Challacombe, P. M. W. Gill, B. Johnson, W. Chen, M. W. Wong, C. Gonzalez, J. A. Pople, Gaussian, Inc., Wallingford CT, **2004**.

Received: January 23, 2012
Revised: March 8, 2012

Slippery characters: The 7-(thien-2-yl)benzotriazinyl radical packs in 1D columns with alternate short and long interplanar distances. Slippage of radicals along the stacking direction causes the near orthogonality of their singly occupied molecular orbitals and therefore leads to ferromagnetic interactions between them (see figure).

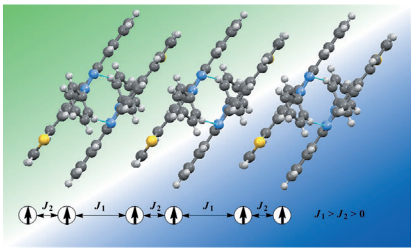

Magnetic Properties

*C. P. Constantinides, P. A. Koutentis,**
J. M. Rawson .... ■■■■–■■■■

Ferromagnetic Interactions in a 1D Alternating Linear Chain of π-Stacked 1,3-Diphenyl-7-(thien-2-yl)-1,4-dihydro-1,2,4-benzotriazin-4-yl Radicals